*J. Fluid Mech.* (2004), *vol.* 514, *pp.* 65–75. © 2004 Cambridge University Press 
DOI: 10.1017/S0022112004000114 Printed in the United Kingdom

# Rapid temporal acceleration of a turbulent pipe flow

By DAVID GREENBLATT† AND EDWARD A. MOSS

School of Mechanical Engineering, University of the Witwatersrand, Private Bag 3, WITS 2050, South Africa

(Received 22 October 2002 and in revised form 4 May 2004)

Measurements were made of fully developed turbulent pipe flows subjected to temporal pressure gradients larger than those considered previously. Integral profile parameters exhibited similar qualitative trends when time was scaled with the flow rise time and this differed from corresponding spatial development of flows subjected to steady streamwise pressure gradients. Velocity profiles were initially characterized by significant reduction of their wake component. This was accompanied by turbulence intensity freezing in the core region of the pipe and a rapid turbulence increase in the near-wall region that propagated towards the pipe centre. The final phase of the acceleration was characterized by reconstitution of the wake, producing a velocity profile inflection and the generation of turbulence in that vicinity. These features were not observed in previous investigations, possibly due to the present use of higher ramp rates and initial Reynolds numbers.

## 1. Introduction

Pulsatile turbulent pipe and tube flows, which oscillate about a non-zero mean, are common in fluid machinery and biological systems. Experimentally, these flows are analysed and categorized on the basis of an appropriate frequency parameter (see e.g. Ramaprian & Tu 1983). Prediction methods, however, employ turbulent models, which are developed and optimized for steady flows, in unsteady formulations (e.g. Scotti & Piomelli 2002). As such, parameter-based empirical generalizations do not enter explicitly into these formulations. Moreover, it is implicitly assumed that homogenous temporal and inhomogeneous spatial pressure gradients have an equivalent effect on the Reynolds stresses. It is not surprising, therefore, that turbulence quantities and wall shear stress are poorly predicted.

An experimental approach to assist in resolving this impasse is to study transient (temporally accelerated or decelerated) flows, thereby removing frequency as a parameter. This also avoids complications associated with assessing the effects of an acceleration that immediately follows a deceleration and vice versa. Temporally accelerated flows have a steady counterpart exemplified by spatially (streamwise) accelerated boundary layers, i.e. those subjected to favourable spatial pressure gradients. When spatial pressure gradients are large, the flow exhibits significant departures from standard turbulent laws and can even tend asymptotically to a laminar state (e.g. Sreenivasan 1982; Warnack & Fernholz 1998). For unsteady turbulent flows, investigations have been conducted by Maruyama, Kuribayashi &

† Present address: Flow Physics and Control Branch, NASA Langley Research Center, Hampton, VA 23681-2199, USA.

https://doi.org/10.1017/S0022112004000114 Published online by Cambridge University Press

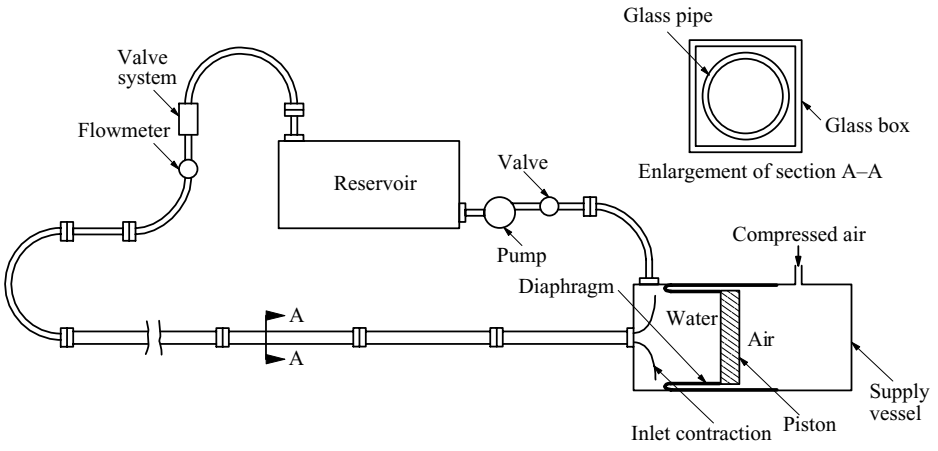



FIGURE 1. Schematic of test facility.

Mizushina (1975) and He & Jackson (2000). In the former investigation, unsteady flow development was studied, following a 'stepwise' increase in flow rate. Turbulence was generated initially in the near-wall region and subsequently propagated towards the centre of the pipe. The latter more detailed investigation, involving ramp-up type increases in velocity, identified delays associated with turbulence production, energy redistribution and radial propagation of turbulence. Both of these investigations, however, relied on a static head of liquid to achieve the ramp-up acceleration. Consequently, both achieved relatively low ramp rates [$\alpha \equiv d^3/\nu^2(\mathrm{d}\bar{U}/\mathrm{d}t) < 70 \times 10^6$] combined with low initial Reynolds numbers ($Re_0 \leqslant 7000$), and even lower $\alpha$ with increasing $Re_0$. In addition, both investigations employed relatively sparse measurements across the pipe radius, with typically 12 or less measurement locations.

The present experimental investigation considers the rapid temporal ramp-up acceleration and relaxation of a streamwise-fully-developed turbulent pipe flow. Detailed measurements of the temporally developing flow profiles were made with a single-component laser-Doppler velocimeter (LDV). Deficiencies present in the above-mentioned ramp-up investigations, such as low ramp rates, low $Re_0$, and low radial measurement resolution, were addressed.

## 2. Experimental setup

Experiments were performed on a pipe-flow facility, with water as the working fluid (see figure 1). The facility comprised eight 1.5 m long sections of high-accuracy glass piping, of internal diameter $d = 48$ mm (radius $a = d/2$), joined together smoothly by means of Teflon sleeves. A large pressurized vessel supplied water to the piping via a bell-mouth entrance contraction. Primary measurements were made in the horizontal plane of the piping by means of a single component LDV. Each pipe was enclosed in a glass, water-filled, box to reduce optical refraction (see figure 1) and thus measurements could be made at arbitrary locations along the length of the piping. The section of piping furthest downstream was connected to plastic tubing that incorporated a magnetic flow meter for monitoring the instantaneous cross-sectional velocity $\bar{U}(t)$. The plastic tubing also incorporated a valve system with a computer-controlled pneumatically operated valve that was located further downstream. Water exited the valve, via additional tubing, to a reservoir, from where it was pumped back to the supply vessel.

https://doi.org/10.1017/S0022112004000114 Published online by Cambridge University Press

| Case no. | $p^+$ | $k \times 10^6$ | $\Lambda$ | $\alpha \times 10^{-6}$ |
|---|---|---|---|---|
| 1 | 0.012 | 1.7 | 10 | 81 |
| 2 | 0.019 | 2.8 | 17 | 143 |
| 3 | 0.045 | 5.8 | 42 | 320 |

TABLE 1. Estimates of maximum values of parameters associated with the temporally accelerated turbulent pipe-flow.

Temporal accelerations were achieved by initially establishing a steady turbulent flow and then opening the pneumatically operated downstream valve in a ramp-type fashion. In order to achieve large temporal pressure gradients (high ramp rates) the supply vessel was subjected to a constant pressure equivalent to a 10 m head of water. Pressure gradients of varying severity were achieved by varying the rate at which the pneumatic valve opened (see § 3). When a desired pressure gradient was achieved, time-dependent velocity profiles $U(r, t)$ and turbulence fluctuations $u'(r, t)$ were obtained by ensemble-averaging repeated experimental runs within 50 ms time windows (cf. He & Jackson 2000), at approximately 25 radial locations, located at 190 diameters downstream of the entrance contraction (the test location). Sufficient data were acquired at all locations to ensure less than 1% uncertainty based on 95% confidence intervals.

Magnetic flow-meter data and integrated cross-sectional LDV velocities differed by no more than 0.5%. For all cases considered, the initial Reynolds number ($Re_0$), was set at approximately 31 000, with a final value of $Re_1 = 82\,000$ after the acceleration. Due to the excessively large number of runs required to offset low LDV data rates near the wall, the vast majority of velocity profiles were confined to radial locations $Y_0^+ > 20$. Selected data were acquired at $Y_0^+ < 12$ for wall shear-stress estimates. Additional steady profiles at $Re_0 = 31\,000$ were acquired at $100d$ upstream of the test location, where $100d > \int \bar{U}\,\mathrm{d}t$ for the duration of each experiment. This ensured that the observations made at the test location were streamwise-independent temporal variations and not washed-down upstream effects.

## 3. Discussion of results

Three experiments were performed, where the imposed pressure gradients corresponded to those that bring about known responses in spatially accelerated turbulent boundary layers (see table 1): namely, the maintenance of local equilibrium (case 1), the breakdown of local equilibrium (case 2), and relaminarization (case 3) (see Sreenivasan 1979). Pressure gradient severity was assessed by considering the unsteady forms of three commonly used steady pressure-gradient parameters: $p^+ \equiv -(\nu/\rho U_\tau^3)\,\mathrm{d}p/\mathrm{d}x$, $k \equiv -(\nu/\rho \bar{U}^3)\,\mathrm{d}p/\mathrm{d}x$ and $\Lambda \equiv -(a/\tau_w)\,\mathrm{d}p/\mathrm{d}x$ (e.g. Narasimha & Sreenivasan 1979). Maximum values corresponding to the three cases were estimated by assuming that $\rho\,\mathrm{d}\bar{U}/\mathrm{d}t \approx -\mathrm{d}p/\mathrm{d}x$, and $\tau_w$ was estimated using the law of the wall (cases 1 and 2) and near-wall velocity profiles (case 3).

To provide a common basis for comparing the various cases, time was non-dimensionalized with respect to a virtual starting time $t_0$ and a rise time $T$ (i.e. $t^* \equiv (t - t_0)/T$) by matching normalized values of $\alpha$ at the beginning and end of each acceleration. The resulting variations of $\bar{U}$ with $t^*$ are shown in figure 2, where $T = 3$, 1.62 and 0.85 s for cases 1, 2 and 3, respectively. The maximum values

https://doi.org/10.1017/S0022112004000114 Published online by Cambridge University Press

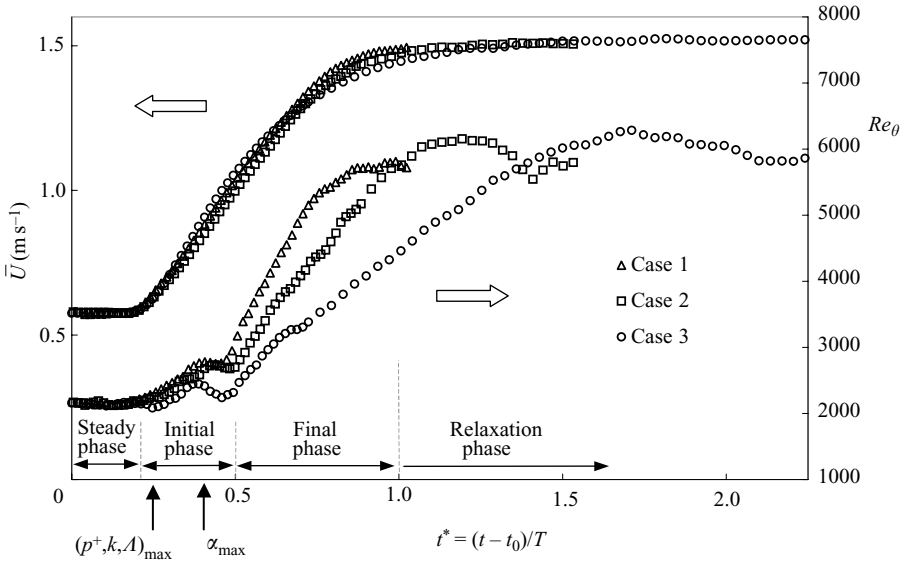



FIGURE 2. Variations of cross-sectional mean velocity and momentum-thickness Reynolds number with dimensionless time.

$p^+_{max}$, $k_{max}$ and $\Lambda_{max}$ occur soon after commencement of the acceleration at $t^* \approx 0.25$ and $\alpha_{max}$ occurs later at $t^* \approx 0.4$ as shown on the figure. The ramp-up is conveniently divided into four different phases (figure 2): a *steady phase*, prior to the ramp-up where $\alpha \approx 0$; an *initial phase*, extending from when $\alpha > 0$ to $t^* \leqslant 0.5$; a *final phase* $(0.5 < t^* \leqslant 1)$; and a *relaxation phase* $(t^* > 1)$.

Integral effects of the acceleration were assessed by considering time-dependent displacement thickness ($\delta^*$), momentum-thickness Reynolds number ($Re_\theta \equiv \bar{U}\theta/\nu$) and shape factor ($H \equiv \delta^*/\theta$), defined for axisymmetric flows. For all cases, the ramp-up brings about reductions in $\delta^*$ (figure 3) during the initial phase, and these reductions increase with increasing ramp rate. In all cases, $\delta^*$ reaches a minimum at $t^* \approx 0.5$, although the physical time taken to reach this minimum clearly decreases with increasing ramp rate. During the initial phase, $\delta^*$ and $Re_\theta$ (figure 2) variations associated with case 3 deviate markedly from those associated with cases 1 and 2. However, all shape factors $H$ (figure 3) exhibit a local minimum, followed by a local maximum that corresponds to the minimum $\delta^*$. The local minima each correspond to a kink in $\delta^*$ that occurs approximately halfway through the initial phase and are associated with $\bar{U}$ inflection (or $\mathrm{d}\alpha/\mathrm{d}t = 0$) at $t^* \approx 0.4$ (see figure 2). For $t^* > 0.4$, all boundary layers become thinner at a faster rate, e.g. $|\mathrm{d}\delta^*/\mathrm{d}t^*|$ increases, and this is particularly evident in case 3 where $Re_\theta$ reduces from 2440 to 2240. These trends, which are observed after the acceleration parameters have reached their maximum values, are further elucidated with respect to the velocity profile development discussed below.

During the early part of the final phase $(0.5 < t^* < 0.75)$, the dimensionless recovery rates for $\delta^*$ and $Re_\theta$, are inversely proportional to the magnitude of the acceleration, but the $H$ variations for the three cases are qualitatively similar. The similarity in $H$ for $0 \leqslant t^* \leqslant 0.75$ is noteworthy, as it shows that its behaviour in the dimensionless framework is virtually independent of acceleration rate. For $t^* > 0.75$, integral quantities associated with case 1 recover much sooner, in a dimensionless sense,

https://doi.org/10.1017/S0022112004000114 Published online by Cambridge University Press

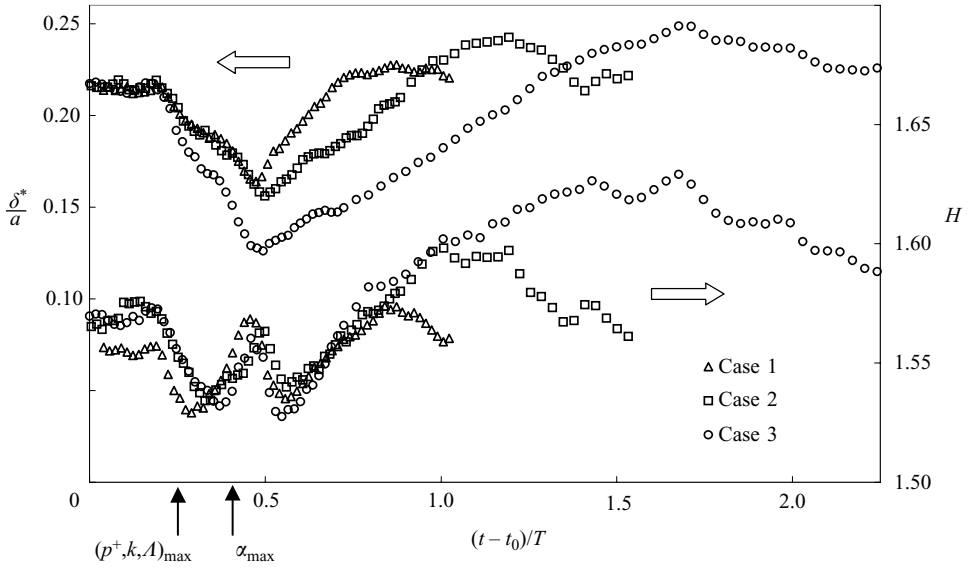



FIGURE 3. Variations of dimensionless displacement thickness and shape factor with dimensionless time.

than those of cases 2 and 3; however recovery rates are approximately equal when the comparison is made on the basis of dimensional time (not explicitly shown).

In spatially relaminarizing flows, velocity profiles progressively adopt a distinctive laminar character, with associated significant reductions in $\delta^*$ and $Re_\theta$. A local minimum in $H$ occurs at approximately the same location as $k_{\max}$, while downstream of this a distinct local $H$ maximum is evident prior to retransition (e.g. Warnack & Fernholz 1998). When the pressure gradient is insufficient to cause relaminarization, the local $H$ maximum is absent (e.g. Fernholz & Warnack 1998). In contrast, for the present time-dependent system (figure 3) $H$ is virtually identical over most of the acceleration irrespective of the pressure gradient ($1.7 \leqslant k_{\max} \leqslant 5.8$). These variations are qualitatively similar to those during spatial relaminarization, but their excursions ($H_{\max} - H_{\min}$) are approximately ten times smaller than their spatial counterparts. Note that the present shape factors should not be compared to $H = 3$ and 2.6 corresponding to steady laminar pipe flow (paraboloid) or boundary layer profiles, but rather those corresponding to temporally accelerated flows. Computations of highly accelerated, initially turbulent, pipe flows (Greenblatt & Moss 1999) showed that the integral flow development is virtually independent of the resulting state of the flow (i.e. laminar or turbulent), and is determined essentially by the pressure gradient severity. Thus the overall trends observed here cannot be explained in terms of the flow state. It should further be noted that marked reductions in $Re_\theta \equiv \bar{U}\theta/\nu$ during steady streamwise acceleration are absent during temporal acceleration, as $Re_\theta$ never falls below its initial value irrespective of the imposed pressure gradient. Finally, note that although these ramp rates are high in the context of unsteady flows, the maximum value of $\Lambda$ (see table 1) is less than the value ($\Lambda \approx 50$) considered necessary for complete relaminarization (Narasimha & Sreenivasan 1979).

During the relaxation phase ($t^* > 1$), all boundary layer parameters exhibit overshoots of their final values. The degree of overshoot is proportional to $\alpha$ and the $t^*$ at which the overshoot occurs increases with increasing $\alpha$. Note, however, that the

https://doi.org/10.1017/S0022112004000114 Published online by Cambridge University Press

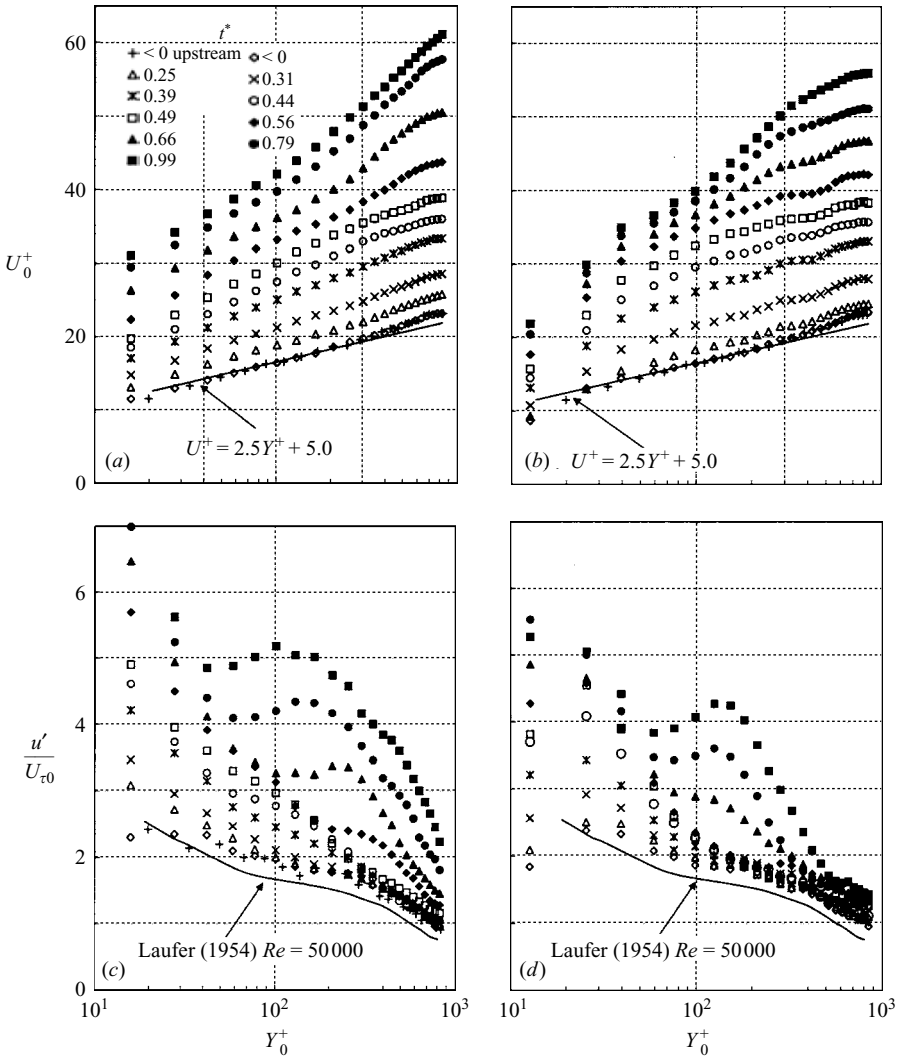



FIGURE 4. Ensemble-averaged velocity and turbulence variations with distance from the wall, scaled according to initial conditions. (*a*, *c*) case 1, $T = 3$ s, (*b*, *d*) case 3, $T = 0.85$ s.

dimensional time taken from the minimum $\delta^*$ to the overshoot maximum is approximately the same for all cases (about 1 s), and this may be related to conditions invariant in the experiment, such as $a/\Delta\bar{U}$. In all cases the boundary layers do not appear to have fully relaxed over the time span of the experiment, as there are still small time-dependent variations in integral parameters at the end of the relaxation phase.

Absolute ensemble-averaged velocity and turbulence profiles (i.e. scaled with respect to initial wall variables $U_0^+ \equiv U/U_{\tau 0}$, $u'/U_{\tau 0}$ and $Y_0^+ \equiv yU_{\tau 0}/\nu$) are shown in figures 4(*a*) to 4(*d*) for cases 1 and 3. Upstream steady profiles are also shown. Conventional scaling is presented in figures 5(*a*) and 5(*b*), but only for $t^* < 0.5$ due to the progressively increasing error associated with the estimation of $U_\tau$ in case 3 (see discussion below). For case 1, shortly after commencement of the acceleration ($t^* \leqslant 0.31$), the wake component of the profile begins to diminish (figures 4*a* and 4*e*). The corresponding turbulence intensity over most of the pipe radius ($Y_0^+ > 200$; $y/a > 0.25$) remains

https://doi.org/10.1017/S0022112004000114 Published online by Cambridge University Press

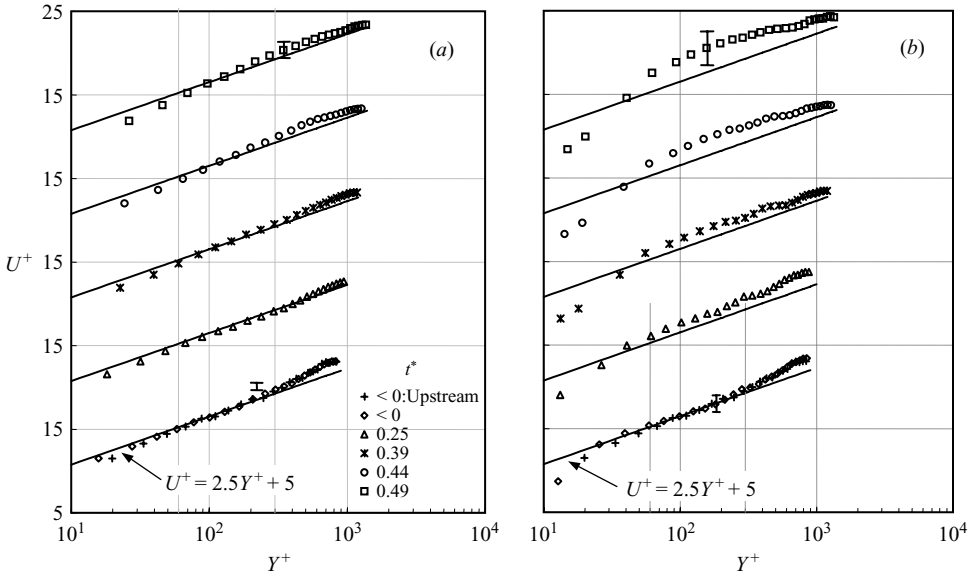



FIGURE 5. Ensemble-averaged velocity and turbulence variations with distance from the wall, using conventional scaling. (*a*) case 1, (*b*) case 3, $t^* < 0.5$.

constant or 'frozen' in its pre-accelerated state, but increases sharply with time near the wall (figure 4*c*). For $0.31 < t^* < 0.44$ the turbulence continues increasing near the wall and propagates inwards, from the wall towards the centre of the pipe, although in the core region (approximately defined by $Y_0^+ > 300$, $y/a > 0.37$), the turbulence remains effectively frozen. The velocity profile continues to deviate from its standard steady-state shape and at $t^* \approx 0.44$ the wake region is distorted and significantly reduced, corresponding to the minimum $\delta^*$ and maximum $H$ described previously (see figures 2 and 3). This reduction of the wake is consistent with the observed increase in $|\mathrm{d}\delta^*/\mathrm{d}t^*|$ for $0.38 \leqslant t^* \leqslant 0.46$ shown in figure 3, despite the fact that the ramp rate and pressure gradient parameters are decreasing. At $t^* \approx 0.49$, turbulence in the core region begins to increase in an approximately uniform manner while, simultaneously, a 'kink' forms in the velocity profile at $Y_0^+ \approx 600$.

For $0.5 < t^* < 1$, the velocity profile is characterized by the regeneration of the wake component, clearly evident at $t^* = 0.56$. During this final phase, while the acceleration diminishes ($\mathrm{d}\alpha/\mathrm{d}t < 0$), the turbulence intensity profile develops in an unusual manner. A dominant feature is the regeneration of turbulence, commencing from $Y_0^+ \approx 300$ at $t^* \approx 0.56$, which then propagates progressively towards the wall. Simultaneously, the near-wall turbulence ($Y_0^+ \approx 15$) and that in the core region increase gradually. The net result is a high level of turbulence close to the wall, consistent with steady flows, and a local peak in the turbulence intensity that propagates towards the wall with time. With increasing time the local peak would be expected to disappear as the profile relaxed to its new steady-state condition, but this was not determined here as case 1 data were not acquired for $t^* > 1$. Examination of the velocity profiles showed that the reconstitution of the wake brings with it an 'inflection region' in the vicinity $Y_0^+ \approx 300$ that is initiated at $t^* \approx 0.56$ (we use the term *inflection region* rather than *inflection point* primarily due to uncertainties associated with differentiating experimental data). As the wake component of the profile continues to grow and propagate towards the wall, so the turbulence peak follows the same trend. Although the current investigation

https://doi.org/10.1017/S0022112004000114 Published online by Cambridge University Press

involves an internal flow, this phenomenon is similar to turbulent external flows, such as mixing layers, in which the peak turbulence intensities correspond to the inflection point (see for example Oster & Wygnanski 1982). Note, however, that this is a qualitative comparison, since the present inflection points are not as clearly defined as those in mixing layers.

For case 2 (not shown), velocity profiles were similar despite the larger pressure gradient ($p^+ > 0.015$) and the main difference was that the velocity profile kink occurred earlier ($t^* \approx 0.44$) and closer to the wall ($Y_0^+ \approx 500$). The turbulence intensity also behaved in a similar manner to that of case 1, with extended turbulence freezing in the core region of the pipe, which remained constant for $Y_0^+ > 300$ until $t^* = 0.5$. The wake trends were similarly delayed and the corresponding turbulence peak was closer to the wall.

In case 3 (figure 4*b*) the kink observed previously occurred much earlier and yet closer to the wall ($Y_0^+ \approx 300$). The logarithmic and wake regions are distorted with increasing time to such an extent that two velocity plateaux are evident: one at $200 < Y_0^+ < 400$ and the other at $700 < Y_0^+ < 800$ ($t^* = 0.49$). Simultaneously, turbulence is frozen at $Y_0^+ > 150$ for the entire initial phase (figure 4*d*). In a manner consistent with the trends of the previous two cases, the developments during the final phase of the acceleration occur later in a non-dimensional sense (discussed further below). There is also relatively little velocity increase in the region originally associated with the logarithmic profile as can be seen by comparing cases 1 and 3 for $Y_0^+ < 300$. The associated local turbulence intensity maximum is initiated close to the wall, at $Y_0^+ \approx 120$, but does not propagate towards the wall for the remainder of the final phase. This should be contrasted with cases 1 and 2, where initially turbulence is generated at $Y_0^+ \approx 300$ and 200, respectively, and then propagated to $Y_0^+ \approx 120$ in both cases at the end of the acceleration.

When conventional scaling is used (figure 5*b*), the profile exhibits a log-law overshoot for $t^* < 0.5$ as a result of the low wall shear stress. Unfortunately, progressively increasing errors associated with wall shear-stress estimates, based on a comparison of the steady flows with Blasius's equation, precluded meaningful assessment of the data for $t^* > 0.5$.

The present observations appear to contradict the findings of Maruyama *et al.* (1976) and He & Jackson (2000), who observed the generation of turbulence near the wall that propagated radially towards the pipe centre. While in the current instance this is true during the initial phase (i.e. for $t^* \leqslant 0.5$), the dynamics are completely transformed by the regeneration of the wake and the associated local turbulence peak. There are three plausible, but not mutually exclusive, explanations for these differences. Firstly, the ramp rates employed by the above-mentioned investigators were significantly lower than those employed here. Secondly, the initial Reynolds numbers in those investigations were low, i.e. 5000 and 7000 respectively. Thus low Reynolds number artifacts may have masked the resulting the profile development. Thirdly, their radial resolution in the near-wall region may not have been high enough to reveal the level of detail reported here. Note, in addition, that the upstream state of the flow was not reported in either of those investigations.

In order to quantify near-wall turbulence generation during the initial phase, dimensionless time ($t^*$) corresponding to $(u' - u'_0)/u'_0 > 0.15$ was plotted as a function of its absolute distance from the wall $Y_0^+$, giving an indication of the time taken for turbulence to propagate across the pipe from the wall (see figure 6). Note that the location $Y_0^+ \approx 20$ was the closest to the wall at which turbulence measurements were acquired for all three cases. The figure indicates that higher acceleration rates

https://doi.org/10.1017/S0022112004000114 Published online by Cambridge University Press

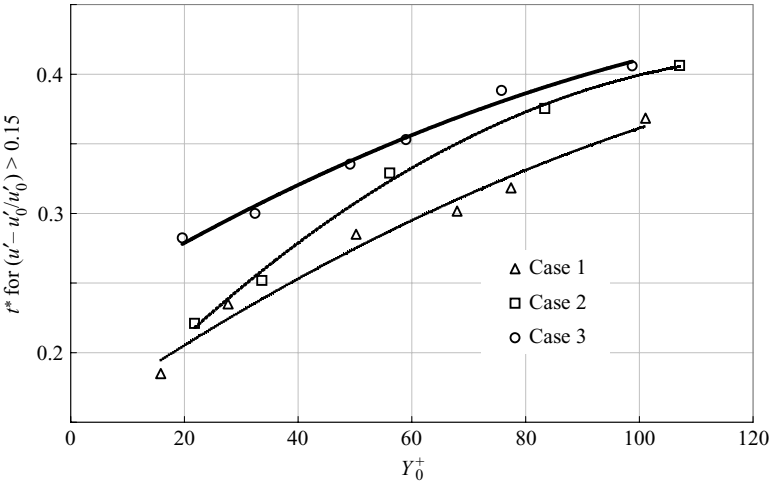



FIGURE 6. Dimensionless time for which $(u' - u'_0)/u'_0 > 0.15$, as a function of wall distance scaled with initial conditions.

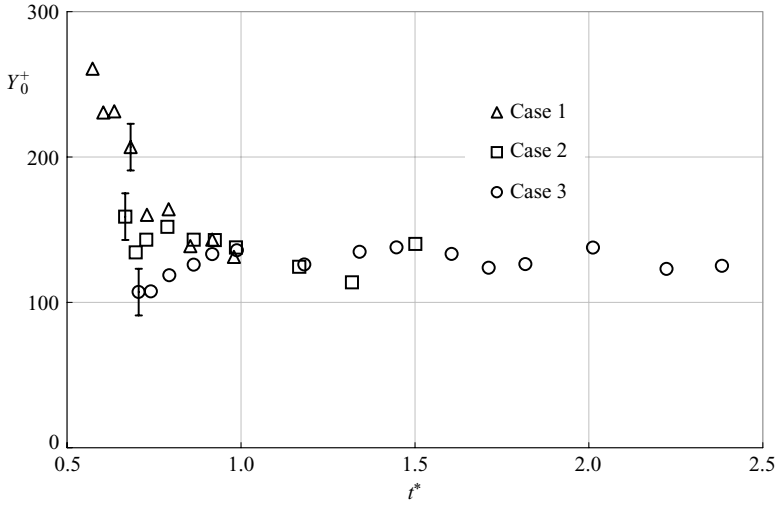



FIGURE 7. Locations and times at which discernible turbulence intensity peaks occur.

are associated with longer delays in near-wall turbulence regeneration. According to the above criterion ($(u' - u'_0)/u'_0 > 0.15$), turbulence regenerates at $t^* \approx 0.19$, 0.22 and 0.28 for cases 1, 2 and 3, respectively. Following initial regeneration, the turbulence propagates at approximately the same rate for all cases and given the experimental uncertainly, it cannot be discerned if the propagation rate is affected by the acceleration. At some time, that is dependent upon acceleration rate, experimental uncertainty precludes discernment of further turbulence propagation and thus the process effectively ceases at $t^* \approx 0.4$.

Subsequent to the process discussed above, turbulence during the final phase of the acceleration begins to regenerate at some location away from the wall. For purposes of quantification and comparison, the location and time corresponding to discernible peaks in $u'$ are plotted in figure 7. The figure shows that turbulence peaks appear soonest for the milder acceleration ($t^* \approx 0.57$ for case 1) and progressively later for

https://doi.org/10.1017/S0022112004000114 Published online by Cambridge University Press

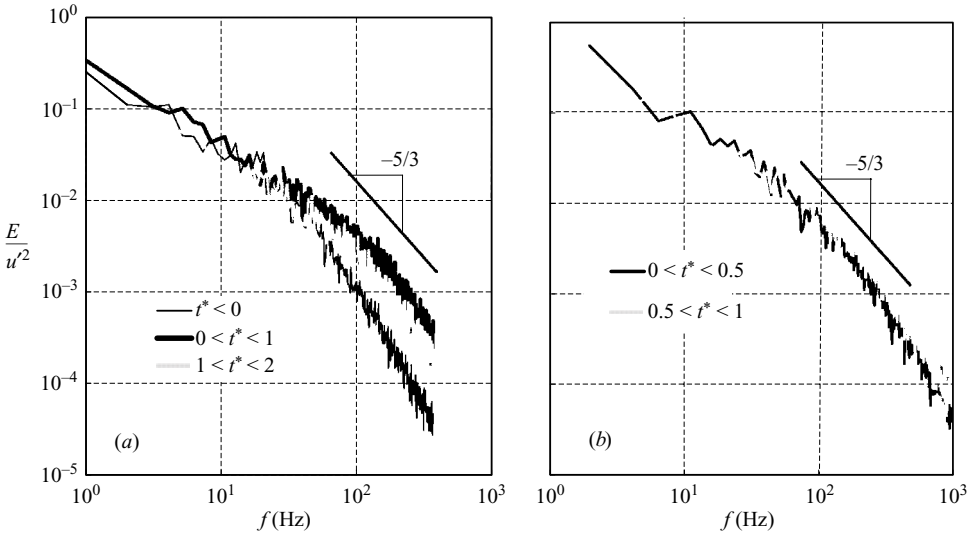



FIGURE 8. Turbulence spectra before, during and after the flow acceleration for case 3. $Y_0^+ = 152$.

the more severe accelerations ($t^* \approx 0.67$ and 0.71 for cases 2 and 3, respectively). This is because the wake reconstitution during the final phase of the acceleration occurs soonest for case 1, and hence the accompanying turbulence generation associated with the inflectional region occurs earliest. The turbulence peak associated with case 1 moves towards the wall with increasing time, while that associated with case 3 propagates slightly away from the wall. At the end of the final phase of the acceleration, all peaks tend towards the same location, namely $Y_0^+ \approx 130$, although the reason for this is not clear. For all cases considered the turbulence profiles have not fully relaxed to their steady unperturbed state.

It was considered prudent to investigate the possible existence of a preferred frequency or frequencies associated with the turbulence generation process. To achieve this, turbulent spectra were measured before, during, and after the acceleration. For data analysed during the acceleration, ensemble-averaged velocities of the experiment were subtracted from the instantaneous LDV velocity–time data for 50 repetitions of the experiment. An example, measured at $Y_0^+ \approx 150$ (the approximate vicinity of turbulence regeneration) for case 3 is presented in figure 8(*a*), for $t^* < 0$ (i.e. steady flow prior to the acceleration), $0 \leqslant t^* \leqslant 1$ (during the acceleration) and $t^* > 1$ (subsequent to the acceleration). All spectra are non-dimensionalized with respect to the average turbulence intensity in the time interval under consideration. All spectra show similar behaviour, in accordance with the $-5/3$ law and there does not appear to be a preferred frequency associated with the generated turbulence. Spectra were also considered for the data acquired separately during the initial and final phases, namely $0 \leqslant t^* \leqslant 0.5$ and $0.5 < t^* \leqslant 1$ (figure 8*b*). When non-dimensionalized with respect to the average turbulence intensity within each time interval as before, the spectra are virtually identical. There was thus no evidence of a preferred frequency associated with the turbulence regeneration.

The authors would like to thank Drs A. H. Abbot and D. F. da Silva for assistance in performing these experiments.

https://doi.org/10.1017/S0022112004000114 Published online by Cambridge University Press

## REFERENCES


Fernholz, H. F. & Warnack, D. 1998 The effects of a favourable pressure gradient and of the Reynolds number on an incompressible axisymmetric turbulent boundary layer. Part 2. The boundary layer with relaminarization. *J. Fluid Mech.* **359**, 329–356.

Greenblatt, D. & Moss, E. A. 1999 pipe-flow relaminarization by temporal acceleration. *Phys. Fluids* **11**, 3478–3481.

He, S. & Jackson, J. D. 2000 A study of turbulence under conditions of transient flow in a pipe. *J. Fluid Mech.* **408**, 1–38.

Laufer, J. 1954 The structure of turbulence in fully developed pipe flow. *NACA Rep.* 1174, pp. 1–18.

Maruyama, T., Kuribayashi, T. & Mizushina, T. 1976 The structure of the turbulence in transient pipe flows. *J. Chem. Engng Japan* **109**, 431–439.

Narasimha, R. & Sreenivasan, K. R. 1973 Relaminarization in highly accelerated turbulent boundary layers. *J. Fluid Mech.* **61**, 417–447.

Oster, D. & Wygnanski, I. 1982 The forced mixing layer between parallel streams, *J. Fluid Mech.* **123**, 91–130.

Ramaprian, B. R. & Tu, S. W. 1983 Fully developed periodic turbulent pipe flow. Part 2. The detailed structure of the flow. *J. Fluid Mech.* **137**, 59–81.

Scotti, A. & Piomelli, U. 2002 Turbulence models in pulsating flows. *AIAA J.* **40**, 537–540.

Sreenivasan, K. R. 1982 Laminarescent, relaminarizing and retransitional flows. *Acta Mechanica* **44**, 1–48.

Warnack, D. & Fernholz, H. F. 1998 The effects of a favourable pressure gradient and of the Reynolds number on an incompressible axisymmetric turbulent boundary layer. Part 1. The turbulent boundary layer. *J. Fluid Mech.* **359**, 329–356.


https://doi.org/10.1017/S0022112004000114 Published online by Cambridge University Press